Applied Physics Letters

Shrink induced nanostructures for energy conversion efficiency enhancement in photovoltaic devices

Cite as: Appl. Phys. Lett. **103**, 023104 (2013); https://doi.org/10.1063/1.4812184
Submitted: 11 February 2013 . Accepted: 31 May 2013 . Published Online: 09 July 2013

Bo Zhang, Min Zhang, Keping Song, Qiao Li, and Tianhong Cui

View Online Export Citation CrossMark

ARTICLES YOU MAY BE INTERESTED IN

Low-cost shrink lithography with sub-22 nm resolution
Applied Physics Letters **100**, 133113 (2012); https://doi.org/10.1063/1.3697836

An ultrasensitive and low-cost graphene sensor based on layer-by-layer nano self-assembly
Applied Physics Letters **98**, 073116 (2011); https://doi.org/10.1063/1.3557504

Highly stretchable wrinkled gold thin film wires
Applied Physics Letters **108**, 061901 (2016); https://doi.org/10.1063/1.4941439

Lock-in Amplifiers up to 600 MHz
starting at $6,210
Zurich Instruments
Watch the Video

© 2013 AIP Publishing LLC.

AIP Publishing

Shrink induced nanostructures for energy conversion efficiency enhancement in photovoltaic devices

Bo Zhang, Min Zhang, Keping Song, Qiao Li, and Tianhong Cui[a)]
Department of Mechanical Engineering, University of Minnesota, 111 Church Street S.E., Minneapolis, Minnesota 55455, USA

(Received 11 February 2013; accepted 31 May 2013; published online 9 July 2013)

There will be a huge impact on development of photovoltaics if the energy conversion efficiency (ECE) can be further enhanced using low-cost strategy, because ECE promotion under the promise of low-cost is very challenging. Here we show a simple, controllable, and low-cost approach to create wrinkles and nanogaps on a shrink polymer substrate as a photocathode, demonstrating an ECE enhancement of 34% in dye-sensitized solar cells (DSSCs). The wrinkles and nanogaps can be generated based on the stress mismatch between surface coated nanomaterials and shrink polymer substrate during heat shrink process. With the assistance of shrink induced nanostructures on light trapping and manipulation, the incident photon to current conversion efficiency of DSSCs is greatly enhanced. We anticipate that the controllable shrink induced nanostructures represent a general low-cost approach to accelerate the development of photovoltaic devices with higher ECE.
© *2013 AIP Publishing LLC*. [http://dx.doi.org/10.1063/1.4812184]

The developments of solar cell are attracting more and more attentions due to requirements of preserving non-renewable energy and lowering carbon dioxide emissions.[1,2] Among numerous types of solar cells, dye-sensitized solar cells (DSSCs) can provide lower cost and potentially higher efficiency because of their simple structure and high internal quantum efficiencies.[3–5] However, the DSSCs have some inherent drawbacks, such as fast recombination and slow carrier diffusion, resulting in lower energy conversion efficiency (ECE) compared with silicon based solar cell.[6] Recently, various light manipulation approaches have been proposed to enhance the ECE of photovoltaic devices according to introducing micro/nanostructures such as strips,[7] nanowires,[8,9] pyramids,[10] etc. Appropriate design of micro/nanostructures is capable of increasing the light absorption by increasing the internal scattering of incident light[11] and introducing near-field surface plasmonic evanescent waves.[12] Thus, the ECE of photovoltaic devices will be effectively enhanced. Despite several lithographic techniques including electron beam, ion beam, and nanoimprint enable the precise fabrication of micro/nanoscale patterns,[13,14] the inevitable higher cost introduced by these lithographic techniques will weaken the most significant cost advantages brought by DSSC compared with silicon based photovoltaics.

Metal wrinkles and nanogaps are natural responses to the stress mismatch between thin films of metal and shrink polymer substrates during heat shrink process. It can be easily extended to large area at very low-cost.[15] Flexible photodiodes,[16] transistor arrays,[17] and solar cell systems[18] have been successfully demonstrated by using these low-cost wrinkles. Although the mechanical properties of these devices present an enhancement on wrinkled surfaces, the effects of the wrinkles and nanogaps on the ECE of DSSC have not been explored. In addition, most efforts have been focused on photoanodes in DSSC, leaving the photocathodes of DSSC a lot of unexplored spaces where may offer new paths to enhance the ECE of DSSC. Therefore, we investigated the properties of DSSC with wrinkles and nanogaps on the photocathodes based on shrink polymer. By simply introducing heat, the shrink stress mismatch between the shrunk polymer substrate and nonshrinkable Pt and ITO films will cause the wrinkles and nanogaps. We report here that these structures can enhance the absorption by light trapping and manipulation, and increase the catalytic surface area of Pt film at the same time. Compared with DSSC constructed on flat photocathode, the shrink polymer based devices exhibit a 34.1% enhancement in ECE after controllably adjusting the feature sizes of shrink induced structures. Specifically, the DSSC fabricated with nanogaps on photocathodes led to a great enhancement of incident photon to current conversion efficiency (IPCE). The glass substrate was also replaced by shrink polymer for photoanodes to form the all-polymer structure of DSSC. By introducing micropillar array in photoanodes and winkles and nanogaps in photocathodes, the ECE can be increased by 59.3% compared to the DSSC without any nanostructures. Because both types of DSSCs exhibit great enhancement of ECE by introducing the shrink induced structures, we expect that the shrink induced structures may be extended to many other types of solar cells, enlarging the application ranges.

Fabrication and light trapping processes are illustrated in Fig. 1. To form the wrinkles and nanogaps, a layer of ITO film followed by a layer of Pt film are sputtered on a polystyrene (PS) sheet. As shown in Fig. 1(a), due to the heat shrinkage of the PS substrates, the stiffer, nonshrinkable bilayer films intend to buckle, generating the wrinkles quickly and simply. The biaxial compressive stress will crack the fragile ITO layer to obtain the nanogaps. First, ITO/Pt layers were deposited on the shrink polymer (Polystyrene, Shrinky-Dinks, Alex Inc.) with an AJA sputter system (Model ATC 2000). Subsequently, the shrink film

[a)]E-mail: tcui@me.umn.edu. Tel: 612-626-1636.

 © 2013 AIP Publishing LLC

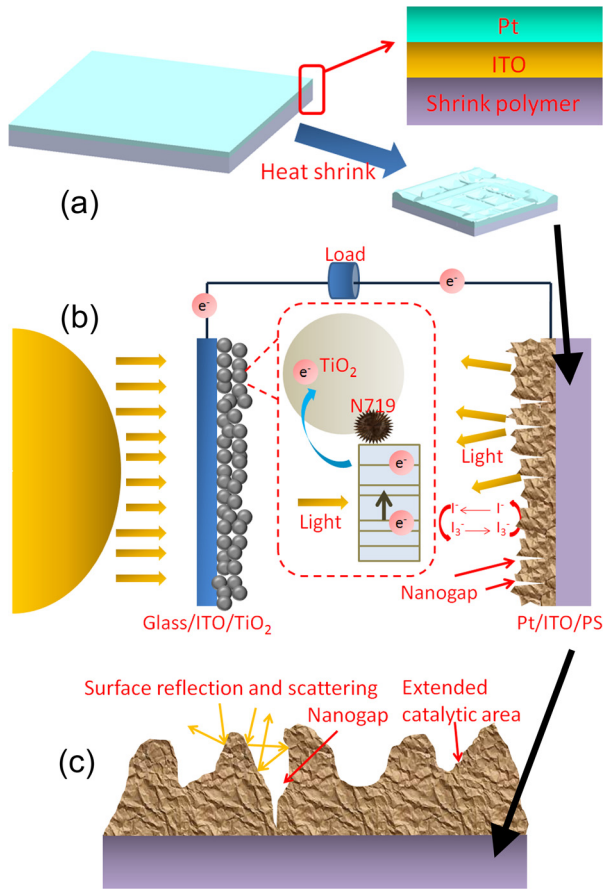

FIG. 1. Schematic diagram of DSSCs with shrink induced wrinkles and nanogaps on the photocathodes. (a) Scheme of the fabrication process of shrink induced wrinkles and nanogaps. The shrink polymer substrate with wrinkles and nanogaps generated on the top surface will serve as photocathode. (b) Scheme of DSSCs incorporating with shrink induced structures. (c) Scheme of the photocathodes utilizing shrink induced wrinkles and nanogaps to enhance the incident light scattering and Pt catalytic area.

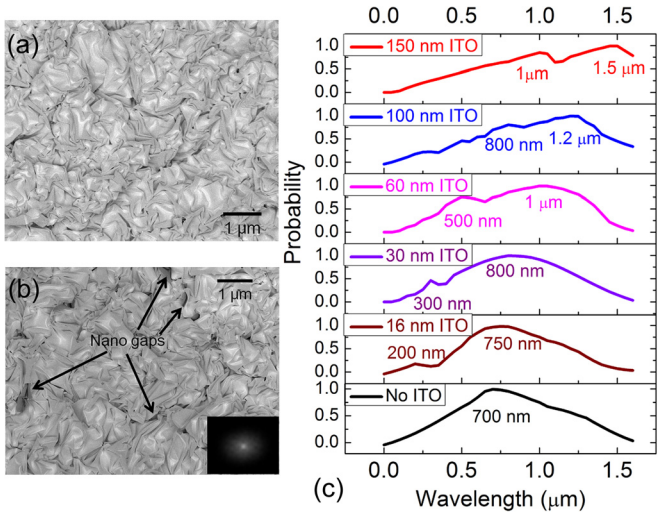

FIG. 2. Quantitative characterization of shrink induced structures on the photocathodes. (a) SEM image of wrinkles generated from shrunk Pt film 50 nm thick without ITO layer. (b) SEM image of wrinkles and nanogaps obtained from shrink ITO/Pt films with 30/50 nm thick. Inset: the disc-shaped 2D FFT pattern, indicating a broad distribution of wavelength in k-space. (c) Wavelength distributions of shrink induced nanostructures are generated from different bilayers with various thickness of ITO layer, but the Pt films are kept as 50 nm thick. The larger wavelength peak represents the wrinkles and the smaller one is for nanogaps. Two spectra peaks are measured by introducing the ITO films, but only one peak appears without ITO film, which confirms that fragile ITO layer causes the nanogaps.

coated with ITO/Pt bilayer was placed in a convection oven (Model 280A) at 150 °C for uniform heating. The substrate was heated to desired temperature in a slowly rising process allowing approximately 5 min and held for 10 min, generating the wrinkle and nanogaps. The wavelength of wrinkles and nanogaps can be controllably generated by simply adjusting the sputtering layer thickness. The wrinkle patterned substrate will serve as photocathode in DSSC, as shown in Fig. 1(b). As shown in Fig. 1(c), the dye molecules cannot absorb incident photons completely, and the residual light is reflected or scattered by the introduced wrinkles and nanogaps on the photocathode, improving the efficiency of light harvesting.

Before characterization of DSSC, the properties of nanostructures caused by heat shrink are investigated. To manipulate the incident light by controlling the wavelength of the wrinkles and nanogaps, several factors, such as the thickness of the thin films, the material properties of the film and PS substrate, play very important roles. Scanning electron microscopy (SEM) images were used to investigate the wrinkles and nanogaps generated by shrink process. The absence of ITO layer will result in only wrinkles by shrinkage of Pt film (Fig. 2(a)), and the fragile ITO layer will introduce the nanogaps by the cracks after shrinking (Fig. 2(b)). To quantitatively analyze the feature sizes of wrinkles and nanogaps, the SEM images were treated by a two-dimensional fast Fourier transform program with MATLAB. The disc-shaped power spectral density indicates a broad distribution of wrinkle and nanogap wavelength in k-space (the inset of Fig. 2(b)). As shown in Fig. 2(c), different thickness of ITO layer incorporated with 50 nm Pt film was quantitatively investigated. Two spectra peaks will show up by introducing ITO films, but only one peak appears without ITO film, which confirms that fragile ITO layer causes the nanogaps. The larger wavelength peak represents the wrinkles and the smaller one is for nanogaps. The wavelength and distribution of wrinkles and nanogaps can be easily tuned by simply adjusting the thickness of ITO layer.

After quantitatively analysis of the wavelength of wrinkles and nanogaps, DSSCs based on these nanostructures are characterized. First of all, to investigate the ability of manipulating light of wrinkles and nanogaps in DSSC, we fabricated DSSCs with different nanostructures on the photocathode. Photoanodes were fabricated based on ITO coated glass (thickness, 1.1 mm; IT5-111-25; Nanocs, Inc.) The substrate was cleaned in acetone under ultrasonic condition for 15 min, and then rinsed with water. After blowing dry, a layer of TiO_2 paste (P6-2100-13; Aqua Solutions, Inc.) was coated on the ITO glass plates by doctor blading. After drying for 10 min, the substrate was placed on a hotplate for 30 min at 450 °C. Then, the TiO_2 coated substrate was treated by UV light for 24 h. After that, the substrate was immersed into 0.5 mM N719 dye (703214; Sigma-Aldrich, Inc.) solution in ethanol for 24 h to load the sensitized dye onto the electrode. The photocathodes were prepared from shrink polymer coated with ITO/Pt. By depositing different thickness of ITO and Pt films, various wavelengths of wrinkles and nanogaps were generated by shrink process. The

electrolyte was 50 mM of tri-iodide in methoxypropionitrile purchased from Solaronix Inc. The dye-loaded TiO_2 photoanodes and photocathodes with shrink induced structures were assembled into a DSSC, and sealed with epoxy (1838B/A; 3M Inc.). DSSCs were characterized by using a calibrated AM 1.5 solar simulator (96000; Newport Inc.). The I-V curves of DSSCs were measured by electrochemical station (CHI 630C; CH Instruments Inc.).

We first investigated the effects of different Pt/ITO layers on ECE. After quantitatively analyzing the wavelength distribution of wrinkles and nanogaps as well as the testing results of DSSCs, the optimal enhancement of efficiency can be easily achieved. As shown in Fig. 3(a), the current densities versus voltage characteristics of the DSSCs with different ITO layers demonstrate that the ECE is relative to the different surface profile of photocathodes. According to the analysis of surface profile of photocathodes, the Pt coated substrate without ITO will have no nanogaps, presenting only 7.04 ± 0.12% efficiency. After introducing nanogaps by depositing ITO layer underneath Pt film, the ECE will rise up to 7.51 ± 0.18% at ITO 30 nm thick, and then drop along with the increasing of ITO thickness. We also kept the ITO with constant 30 nm thick and adjusted the thickness of Pt films. The characterization results also confirm that the photocathode with 30 nm ITO and 50 nm Pt will give the optimal results (Fig. 3(b)). Though the photocathodes have various surface structures generated by different thickness of ITO and Pt, we observed almost the same open-circuit voltage (V_{oc}) of 0.7 V for all the DSSC. However, the short-circuit current density (J_{sc}) presented different responses relative to the surface nanostructures. As shown in Fig. 3(c), the IPCE spectra of DSSCs with certain wavelength of nanostructure on photocathodes showed the enhancement extending over the wavelength range from 300 to 750 nm.

After optimal ECE is achieved, the factors which influence ECE were investigated. The ECE enhancement can be contributed to the increase of light scattering and/or trapping induced by the textured platinum/ITO back contact, as well as the expended catalytic surface area of Pt film. As shown in Fig. 3(e), the optimal DSSC with Pt/ITO 50/30 nm thick presents 34.1% increase of ECE, compared to DSSC with the flat photocathode. Shrink process will offer 4 times larger Pt catalytic surface area due to reduction by half of the lateral dimension of shrink polymer substrates. Thus, the surface area will be 25% of original area. To investigate the effects of these factors on the enhancement of ECE, we fabricated two groups of samples on a flat substrate. The photoanodes of the two group samples have the same area. The photocathode area of group one was the same as the photoanode area, but the photocathode area of group two was four times as the photoanode area. The second group was to mimic the enlarged catalytic area without introducing any light trapping effect. As shown in Fig. 3(f), we compared the ECE of DSSCs with same photoanodes but different photocathodes area, showing 9.9% ECE enhancement with the enlargement of Pt catalytic area. Therefore, besides the enlarged catalytic area, these shrink induced wrinkles and nanogaps will efficiently improve the ECE by the light scattering effect. The multiple scattering of light will lead to an increasing of optical path length and the optical absorption, thereby increasing the ECE. However, the DSSC with only wrinkles can provide 7.04 ± 0.12% efficiency, compared with 5.60 ± 0.15% efficiency from photocathodes, showing

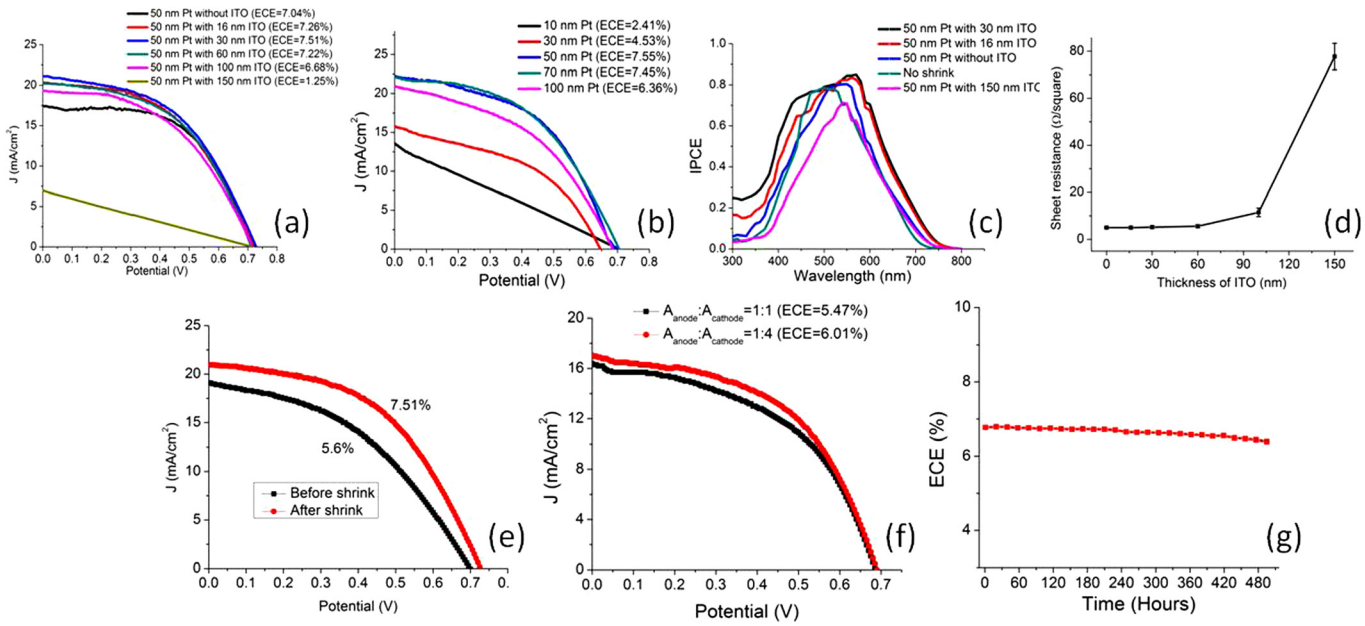

FIG. 3. Characterization of DSSCs with shrink induced structures on photocathodes. (a) The current densities versus voltage characteristics of the DSSCs with various shrink induced nanostructures due to different thickness of ITO layers. The Pt layer was kept as 50 nm thick, but the thickness of ITO film was different. (b) The ITO layer was kept as 30 nm thick, but the thickness of Pt film was different. (c) IPCE spectra of DSSCs with different photocathodes. The wrinkles and nanogaps enable a great IPCE enhancement at incident wavelengths from 300 to 750 nm. (d) Sheet resistance of different thickness of ITO layers with 50 nm Pt film deposited on PS substrate after shrinking. (e) The optimal DSSC with Pt/ITO 50/30 nm thick presents 34.1% increase of ECE compared with DSSC with the flat photocathode. (f) Comparison of DSSCs with same photoanodes but different photocathode area. The ECE shows only 9.9% ECE enhancement after simply enlarging the catalytic area on photocathode. (g) Long term stability characterization of DSSCs. The DSSCs kept 94% of its initial efficiency after 500 h at 60 °C under a real irradiance of successive outdoor sunlight soaking.

only 25.7% enhancement in ECE. So the nanogaps are capable of supplying more photon scattering and diffusion between the interfaces. We also measured surface resistance of different textured photocathodes, as shown in Fig. 3(d). The electric qualities are almost the same when there is no nanogap or very small nanogaps (no ITO or very thin layer of ITO). But huge wavelength of nanogaps (thick ITO layer) will introduce large cracks to the electrodes. This will result in larger sheet resistance of electrodes and decrease ECE greatly, as shown in Fig. 3(a). Therefore, the wavelength of nanogaps should be controlled at an optimal level, to achieve greatest light trapping effect with less electric quality decreasing. In addition, we observe the peak of the IPCE spectrum for the conventional sample (no shrink) locates at around 500 nm, which is consistent with previous results using the same type of dye,[19,20] while other samples with textured back contact are red-shifted with respect to the conventional samples. This red-shift is attributed to plasmon resonance effect, which promoted by the structured back contact.[21,22]

The device stability of our best sample was also characterized, shown in Fig. 3(g). Here, the sample was stored under a real irradiance of successive outdoor sunlight soaking for 500 h at 60 °C. The initial ECE of the testing cell are 6.77%. And this cell exhibited a good stability, still keeping 94% of its initial efficiency after 500 h of aging.

Besides conventional structure of DSSCs, all-polymer structures of DSSCs are also studied herein. As shown in Fig. 4(a), we replaced the conventional glass photoanodes with patterned shrink polymer substrate coated with TiO_2 to form all-polymer structure of DSSC, and investigated the enhancement of ECE by the shrink induced structures. It has been proposed to enhance the ECE of DSSC by introducing micro/nanostructures on the photoanodes.[23,24] However, the conventional fabrication methods on glass substrate are very high-cost, compared with the shrink polymer substrate combining with hot embossing process. By shrink processes, shrink polymer is capable of generating high aspect ratio and various feature sizes of microstructures from a single mold by controlling shrink temperatures.[25,26] Here, we fabricated three groups of all-polymer structure DSSCs to investigate the enhancement of ECE, as shown in Fig. 4(b). First, the shrink polymer based photoanodes were fabricated with micropillar arrays (Fig. 4(c)). A silicon mold was fabricated by photolithography and inductively coupled plasma (ICP) dry etching. Next, the patterns were transferred from the silicon mold to the shrink polymer by Maual Pressor (Model Grimco 12-1-HT). Then, the patterns on the shrink polymer were gently polished and removed by sandpaper. Subsequently, the polished shrink polymers were shrunk at 150 °C to obtain high respect ratio micropillar array. After deposition of 100 nm ITO, a layer of TiO_2 paste was blading coated on the patterned shrink polymer substrate, then dried for 30 min at 150 °C followed by UV light treatment for 24 h. The photocathodes and assembly procedure were the same with the fabrication of DSSCs discussed above. The photoanodes of first group of DSSCs constructed on the shrink polymer substrate with micropillar array patterns (the inset of Fig. 4(a)), and the photocathodes were fabricated with wrinkles and nanogaps by shrink process. The second

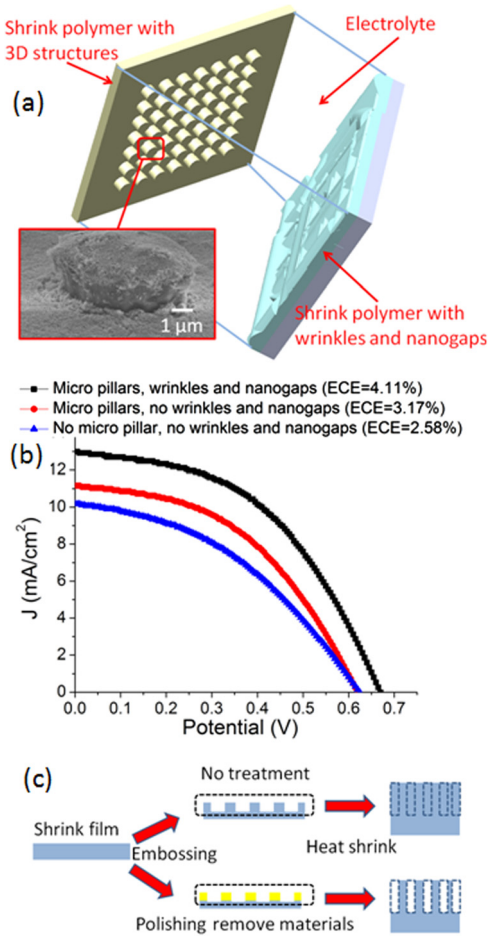

FIG. 4. All-polymer DSSC with shrink induced micro/nanostructures. (a) Scheme of all-polymer DSSC with shrink induced structures on both anode and photocathode. Inset: SEM image of shrink induced micro pillar coated with TiO_2. (b) The current densities versus voltage characteristics of DSSCs with or without shrink induced structures. There is up to 59.3% ECE enhancement of DSSC with shrink induced micro/nanostructures compared with the control group with flat electrodes. (c) Scheme illustration of the formation mechanism of shrink induced micropillar array on the photoanode.

groups of DSSCs had the same photoanodes with the first group, but the photocathodes were flat without any shrink induced structures. The third group was the control group, and both the photoanodes and photocathodes were flat without any shrink induced structures. The control group has only 2.58 ± 0.23% efficiency, and the patterned photoanodes will provide 3.17 ± 0.15% efficiency. The first group is capable of offering up to 4.11 ± 0.18% efficiency, demonstrating 59.3% enhancement of ECE by shrink induced structures on both the photoanodes and photocathodes.

Solar cell market is currently dominated by expensive photovoltaic cells based on silicon substrate. With the development of low-cost solar cells, the DSSC has attracted more and more attentions as an efficient alternative due to its flexibility, low cost, and potential high efficiency. However, the efficiency of DSSC still remains numerous areas for further improvement. Wrinkles and nanogaps on shrink polymer substrates are natural responses to the heat shrink induced stress mismatch of materials and can be easily introduced to large areas in a very low-cost way. By using these shrink induced structures on the photocathodes, the ECE of DSSCs can be enhanced 34.1% due to the increase of light scattering

and/or trapping as well as the enlargement of Pt catalytic surface area. Moreover, the shrink polymer can also provide low-cost patterns on photoanodes, demonstrating all-polymer structure of DSSC with 59.3% enhancement of ECE. We believe these low-cost shrink induced micro/nanostructures enable to extend in many other photovoltaic device applications such as quantum dot solar cells and organic solar cells.

The authors acknowledge the assistance of fabrication and characterization from Nanofabrication Center and the Characterization Facility at the University of Minnesota.

[1]E. H. Sargent, Nature Photon. **6**, 133–135 (2012).
[2]F. C. Krebs, Sol. Energy Mater. Sol. Cells **93**, 394–412 (2009).
[3]A. Hagfeldt, G. Boschloo, L. Sun, L. Kloo, and H. Pettersson, Chem. Rev. **110**, 6595–6663 (2010).
[4]X. Dang, H. Yi, M. Ham, J. Qi, D. Yun, R. Ladewski, M. Strano, P. Hammond, and A. Belcher, Nat. Nanotechnol. **6**, 377–384 (2011).
[5]B. O'Regan and M. Grätzel, Nature **353**, 737–739 (1991).
[6]B. E. Hardin, H. J. Snaith, and M. D. McGehee, Nature Photon. **6**, 162–169 (2012).
[7]Q. Zhang, C. S. Dandeneau, X. Zhou, and G. Cao, Adv. Mater. **21**, 4087–4108 (2009).
[8]M. McCune, W. Zhang, and Y. Deng, Nano Lett. **12**, 3656–3662 (2012).
[9]J. Liao, B. Lei, H. Chen, D. Kuang, and C. Su, Energy Environ. Sci. **5**, 5750–5757 (2012).
[10]H. Pan, J. Qian, Y. Cui, H. Xie, and X. Zhou, J. Mater. Chem. **22**, 6002–6009 (2012).
[11]C. Battaglia, J. Escarre, K. Soderstrom, M. Charrière, M. Despeisse, F. Haug, and C. Ballif, Nature Photon. **5**, 535–538 (2011).
[12]I. Ding, J. Zhu, W. Cai, S. Moon, N. Cai, P. Wang, S. Zakeeruddin, M. Grätzel, M. Brongersma, Y. Cui *et al.*, Adv. Energy Mater. **1**, 52–57 (2011).
[13]V. E. Ferry, M. Verschuuren, H. Li, E. Verhagen, R. Walters, R. Schropp, H. Atwater, and A. Polman, Opt. Express **18**(S2), A237–A245 (2010).
[14]J. Y. Chen and K. W. Sun, Sol. Energy Mater. Sol. Cells **94**, 629–633 (2010).
[15]C. Fu, A.Grimes, M. Long, C. Ferri, B. Rich, S. Ghosh, S. Ghosh, L. Lee, A. Gopinathan, and M. Khine, Adv. Mater. **21**, 4472–4476 (2009).
[16]Y. Sun, W. Choi, H. Jiang, Y. Huang, and J. Rogers, Nature Nanotechnol. **1**, 201–207 (2006).
[17]D. Khang, H. Jiang, Y. Huang, and J. A. Rogers, Science **311**, 208–212 (2006).
[18]J. Kim, P. Kim, N. Pegard, S. Oh, C. Kagan, J. Fleischer, H. Stone, and Y. Loo, Nature Photon. **6**, 327–332 (2012).
[19]S. Hwang, J. Lee, C. Park, H. Lee, C. Kim, C. Park, M. Lee, W. Lee, J. Park, K. Kim, N. Park, and C. Kim, Chem. Commun. **46**, 4887–4889 (2007).
[20]Y. Ren, Y. Zheng, J. Zhao, J. Chen, W. Zhou, and X. Tao, Electrochem. Commun. **16**, 57–60 (2012).
[21]W. Hou, P. Pavaskar, Z. Liu, J. Theiss, M. Aykol, and S. Cronin, Energy Environ. Sci. **4**, 4650–4655 (2011).
[22]N. C. Jeong, C. Prasittichai, and J. T. Hupp, Langmuir **27**, 14609–14614, (2011).
[23]J. S. Bendall, L. Etgar, S. Tan, N. Cai, P. Wang, S. Zakeeruddin, M. Gratzel, and M. Welland, Energy Environ. Sci. **4**, 2903–2908 (2011).
[24]X. Dong, J. Tao, Y. Li, and H. Zhu, Appl. Surf. Sci. **256**, 2532–2538 (2010).
[25]B. Zhang, M. Zhang, and T. Cui, Appl. Phys. Lett. **100**, 133113 (2012).
[26]C. Chen, D. Breslauer, J. Luna, A. Grimes, W. Chin, L. Lee, and M. Khine, Lab Chip **8**, 622–624 (2008).